Luminescence of Lanthanide Ions

in Coordination Compounds and Nanomaterials

Editor **Ana de Bettencourt-Dias**

WILEY

Luminescence of Lanthanide Ions in Coordination Compounds and Nanomaterials

Luminescence of Lanthanide Ions in Coordination Compounds and Nanomaterials

Edited by

ANA DE BETTENCOURT-DIAS

Department of Chemistry, University of Nevada, Reno, USA

WILEY

This edition first published 2014

Registered office
John Wiley & Sons Ltd, The Atrium, Southern Gate, Chichester, West Sussex, PO19 8SQ, United Kingdom

Library of Congress Cataloging-in-Publication Data

Luminescence of lanthanide ions in coordination compounds and nanomaterials
/ edited by Dr Ana de Bettencourt-Dias.
pages cm
Includes bibliographical references and index.
ISBN 978-1-119-95083-7 (cloth)
1. Nanostructured materials. 2. Luminescence. 3. Rare earth
metals–Optical properties. 4. Coordination compounds. I. Bettencourt-Dias, Ana de, editor.
TA418.9.N35L86 2014
546'.41–dc23
2014012258

A catalogue record for this book is available from the British Library.

ISBN: 9781119950837

Set in 10/12 pt TimesLTStd-Roman by Thomson Digital, Noida, India

Contents

List of Contributors

Anthony D'Aléo, CINaM, UMR 7325 CNRS-Aix Marseille Université, France

Chantal Andraud, Laboratoire de chimie, UMR 5281 ENS Lyon-CNRS-Université de Lyon, France

Ana de Bettencourt-Dias, Department of Chemistry, University of Nevada, USA

Jean-Claude G. Bünzli, Swiss Federal Institute of Technology, Switzerland; and Korea University, Republic of Korea

Sarina J. Dorazio, University at Buffalo, State University of New York, USA

Stephen Faulkner, Chemistry Research Laboratory, University of Oxford, UK

Thorfinnur Gunnlaugsson, Trinity College, University of Dublin, Ireland

Olivier Maury, Laboratoire de chimie, UMR 5281 ENS Lyon-CNRS-Université de Lyon, France

David E. Morris, Los Alamos National Laboratory, USA

Janet R. Morrow, University at Buffalo, State University of New York, USA

Gilles Muller, Department of Chemistry, San José State University, USA

Simon J.A. Pope, School of Chemistry, Cardiff University, Wales, UK

Manuel Tropiano, Chemistry Research Laboratory, University of Oxford, UK

Frank C.J.M. van Veggel, Department of Chemistry, University of Victoria, Canada

Preface

The unique spectroscopic properties of the lanthanide ions prompted Sir William Crookes in his lecture delivered 1887 at the Royal Institution to say: "These elements perplex us in our researches, baffle us in our speculations, and haunt us in our very dreams. They stretch like an unknown sea before us – mocking, mystifying, and murmuring strange revelations and possibilities" (*The Chemical News*, 1887, pp. 83–88). These unique properties, which are line-like absorption and equally narrow emission spectra, played a central role in the separation and identification of the 14 elements. As each lanthanide ion shows a characteristic spectroscopic signature and line-like spectra, they have continued to fascinate researchers through the ages and have led to many applications as well as new fields of research. The interest in spectroscopy and spectroscopic applications of the lanthanide ions has resulted in a growing number of publications. Among these are several books that address one or more areas of lanthanide chemistry and spectroscopy, such as the recent *Rare Earth Coordination Chemistry* edited by Chunhui Huang, Wybourne and Smentek's theoretical treatise on the *Optical Spectroscopy of Lanthanides – Magnetic and Hyperfine Interactions*, or *Lanthanide Luminescence* edited by Hänninen and Härmä. Our new book aims to serve scientists whose primary field of interest is spectroscopy and spectroscopic applications of lanthanide ions, veteran scientists for whom the field is reviewed, as well as new scientists, who can find here information that will help them to get started. Finally, this book is also intended as the basis for an intermediate to advanced course in *f* element spectroscopy.

The first two chapters of this work cover theoretical and practical aspects of the emission process, the spectroscopic techniques and the equipment used to characterize the emission. Chapter 3 introduces and reviews the property of circularly polarized emission, while Chapter 4 reviews the use of lanthanide ion complexes in bioimaging and fluorescence microscopy. Chapter 5 covers the phenomenon of two-photon absorption, its theory as well as applications in imaging, while Chapter 6 reviews the use of lanthanide ions as chemosensors. Chapter 7 introduces the basic principles of nanoparticle upconversion luminescence and its use for bioimaging and Chapter 8 reviews direct excitation of the lanthanide ions and the use of the excitation spectra to probe the metal ion's coordination environment in coordination compounds and biopolymers. Finally, Chapter 9 describes the formation of heterobimetallic complexes, in which the lanthanide ion emission is promoted through the hetero-metal.

I am deeply indebted to all who made this book possible. My thanks to the contributing authors of the nine chapters, without whom this book would not have been possible. They are major driving forces in their respective areas and have contributed chapters that are at once excellent tutorials and thorough reviews of their fields. My heartfelt thanks go also to the publisher and everyone involved with the book at Wiley, who, with their continued patience, encouragement, professionalism and enthusiasm led the project to its successful conclusion.

1

Introduction to Lanthanide Ion Luminescence

Ana de Bettencourt-Dias

Department of Chemistry, University of Nevada, USA

1.1 History of Lanthanide Ion Luminescence

After the isolation of a sample of yttrium oxide from a new mineral by Johan Gadolin in 1794, several of the lanthanides, namely praseodymium and neodymium, as well as cerium, lanthanum, terbium and erbium were isolated in different degrees of purity [1]. It was only after Kirchhoff and Bunsen introduced the spectroscope in 1859 as a means of characterising elements that the remaining lanthanides were discovered and the already known ones could be obtained in pure form [2]. Spark spectroscopy provided the means to finally isolate in pure form the remaining lanthanides [3–5]. As will be discussed below, the 4*f* valence orbitals are buried within the core of the ions, shielded from the coordination environment by the filled 5*s* and 5*p* orbitals, and do not experience significant coupling with the ligands. Therefore, the electronic levels of the ions can be described in an analogous way to the atomic electronic levels with a Hamiltonian in central field approximation with electrostatic Coulomb interactions, spin–orbit coupling and finally crystal field and Zeeman effects added as perturbations. All these perturbations lead to a lifting of the degeneracy of the electronic levels and transitions between these split levels are experimentally observed [6]. These transitions, however, are forbidden by the parity rule, as there is no change in parity between excited and ground state. That the emission was nonetheless seen puzzled scientists for a long time [7]. Only when Judd and Ofelt independently proposed their theory of induced electric dipole

Luminescence of Lanthanide Ions in Coordination Compounds and Nanomaterials, First Edition.
Edited by Ana de Bettencourt-Dias.

transitions [8,9] could the appearance of these transitions be satisfactorily explained. As the transitions are forbidden, the direct excitation of the lanthanide ions is also not easily accomplished, and this is why sensitised emission is a more appealing and energy efficient way to promote lanthanide-centred emission. While the ability of the lanthanide salts to emit light was key to their isolation in pure form, sensitised emission was first described by S.I. Weissman only in 1942 [10]. This author realised that when complexes of Eu(III) with salicylaldehyde and benzoylacetonato, as well as other related ligands, were irradiated with light in the wavelength range in which the organic ligands absorb, strong europium-characteristic red emission ensued. Weissman further observed that the emission intensity was temperature and solvent dependent, as opposed to what is seen for europium nitrate solutions [10]. After this seminal work, interest in sensitised luminescence spread through the scientific community, as the potential application of lanthanides for imaging and sensing was quickly recognised [11,12].

1.2 Electronic Configuration of the +III Oxidation State

1.2.1 The 4*f* Orbitals

The lanthanides' position in the fourth period as the inner transition elements of the periodic table indicates that the filling of the 4*f* valence orbitals commences with them. The electronic configuration of the lanthanides is $[Xe]4f^n6s^2$, with notable exceptions for lanthanum, cerium, gadolinium and lutetium, which have a $[Xe]4f^{n-1}5d^16s^2$ configuration. Upon ionisation to the most common +III oxidation state, the configuration is uniformly $[Xe]4f^{n-1}$. La(III) therefore does not possess any *f* electrons, while Lu(III) has a filled 4*f* orbital. While the 4*f* orbitals are the valence orbitals, they are shielded from the coordination environment by the filled 5*s* and 5*p* orbitals, which are more spatially extended, as shown in Fig. 1.1, which displays the radial charge density distribution for Pr(III) [13]. Therefore, lanthanides bind mostly through ionic interactions and the ligand field perturbation upon the 4*f* orbitals is minimal. Nonetheless, as will be discussed below, symmetry considerations imposed by the ligand field affect the emission spectra of the lanthanide ions.

1.2.2 Energy Level Term Symbols

It is usual to describe the configurations of hydrogen-like atoms or ions, that is with only one electron, in terms of the quantum numbers n, l, m_l, s and m_s. In polyelectronic atoms and ions, exchange and pairing energies lead to different configurations, or microstates, with different energies, which are described by new quantum numbers, the total orbital angular momentum quantum number L and its projection along the z axis, the total magnetic orbital angular momentum M_L, and the total spin angular momentum quantum number S, often indicated as the spin multiplicity, $2S+1$, as well as its projection along the z axis, the total magnetic spin quantum number M_S. In the case of heavy elements, such as lanthanides, coupling of the spin and angular momenta is seen, and an additional quantum number, J, the spin–orbit coupling or Russell–Saunders quantum number, is commonly utilised. As will be mentioned below, intermediate coupling for lanthanides is more correct, but the

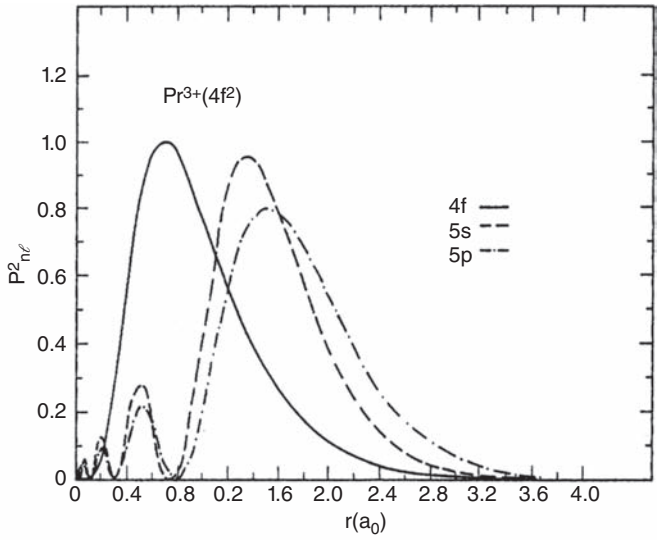

Figure 1.1 *Radial charge density distribution of Pr(III). Reproduced from [13] with permission from Elsevier*

Russell–Saunders formalism is simple to use and will be carried through this chapter. Term symbols with the format $^{2S+1}L_J$, which summarise the quantum number information, are assigned to describe the individual microstates. For a polyelectronic atom or ion with i electrons,

$$L = \sum_i l_i, \quad M_L = -L, \ldots, L$$

$$S = \sum_i s_i, \quad s_i = 1/2$$

and

$$J = L + S, L + S - 1, \ldots, |L - S|.$$

Term symbols can be obtained by determining the microstates, or allowed combinations of all electrons described by quantum numbers, of the atom or ion under consideration and methods to do it is can be found in textbooks [14,15]. Since multiple combinations of electrons are allowed, and therefore many microstates are present, Hund's rules are followed for determination of the ground state. The ground state will have the largest spin multiplicity and the largest orbital multiplicity corresponding to the largest value of L. Finally, if S and L are equal for two states, the ground state will correspond to the largest value of J, if the electron shell is more than half-filled, or an inverted multiplet and the smallest value of J, if the orbital is less than half-filled, which is a regular multiplet. The ground state term symbols for f^n ($n =$ number of electrons in the f shell) configurations are shown in Table 1.1.

Table 1.1 *Ground state term symbols for* f^n *electronic configurations*

Configuration	Term
f^0/f^{14}	$^1S_0$
f^1/f^{13}	$^2F_{5/2}/^2F_{7/2}$
f^2/f^{12}	$^3H_4/^3H_6$
f^3/f^{11}	$^4I_{9/2}/^4I_{15/2}$
f^4/f^{10}	$^5I_4/^5I_8$
f^5/f^9	$^6H_{5/2}/^6H_{15/2}$
f^6/f^8	$^7F_0/^7F_6$
f^7	$^8S_{7/2}$

A complete diagram, showing the ground and excited states of all lanthanide ions in the +III oxidation state with corresponding term symbols, is displayed in Fig. 1.2.

Table 1.2 summarises the most commonly observed emission transitions for the emissive Ln(III) ions.

Table 1.2 *Most common emissive f-f transitions of* Ln^{3+} *[16–28]*

Ln	Transition	λ [nm]
Pr	$^1D_2 \rightarrow {}^3F_4$	1000
	$^1D_2 \rightarrow {}^1G_4$	1440
	$^1D_2 \rightarrow {}^3H_J (J = 4, 5)$	600, 690
	$^3P_0 \rightarrow {}^3H_J (J = 4 - 6)$	490, 545, 615, 640,
	$^3P_0 \rightarrow {}^3F_J (J = 2 - 4)$	700, 725
Nd	$^4F_{3/2} \rightarrow {}^4I_J (J = 9/2 - 13/2)$	900, 1060, 1350
Sm	$^4G_{5/2} \rightarrow {}^6H_J (J = 5/2 - 13/2)$	560, 595, 640, 700, 775
	$^4G_{5/2} \rightarrow {}^6F_J (J = 1/2 - 9/2)$	870, 887, 926, 1010, 1150
Eu	$^5D_0 \rightarrow {}^7F_J (J = 0 - 6)$	580, 590, 615, 650, 720, 750, 820
Gd	$^6P_{7/2} \rightarrow {}^8S_{7/2}$	315
Tb	$^5D_4 \rightarrow {}^7F_J (J = 6 - 0)$	490, 540, 580, 620, 650, 660, 675
Dy	$^4F_{9/2} \rightarrow {}^6H_J (J = 15/2 - 9/2)$	475, 570, 660, 750
	$^4I_{15/2} \rightarrow {}^6H_J (J = 15/2 - 9/2)$	455, 540, 615, 695
Ho	$^5S_2 \rightarrow {}^5I_J (J = 8, 7)$	545, 750
	$^5F_5 \rightarrow {}^5I_J (J = 8, 7)$	650, 965
Er	$^4S_{3/2} \rightarrow {}^4I_J (J = 15/2, 13/2)$	545, 850
	$^4F_{9/2} \rightarrow {}^4I_{15/2}$	660
	$^4I_J (J = 9/2, 13/2) \rightarrow {}^4I_{15/2}$	810, 1540
Tm	$^1D_2 \rightarrow {}^3F_4, {}^3H_4, {}^3F_J (J = 3, 2)$	450, 650, 740, 775
	$^1G_4 \rightarrow {}^3H_6, {}^3F_4, {}^3H_5$	470, 650, 770
	$^3H_4 \rightarrow {}^3H_6$	800
Yb	$^2F_{5/2} \rightarrow {}^2F_{7/2}$	980

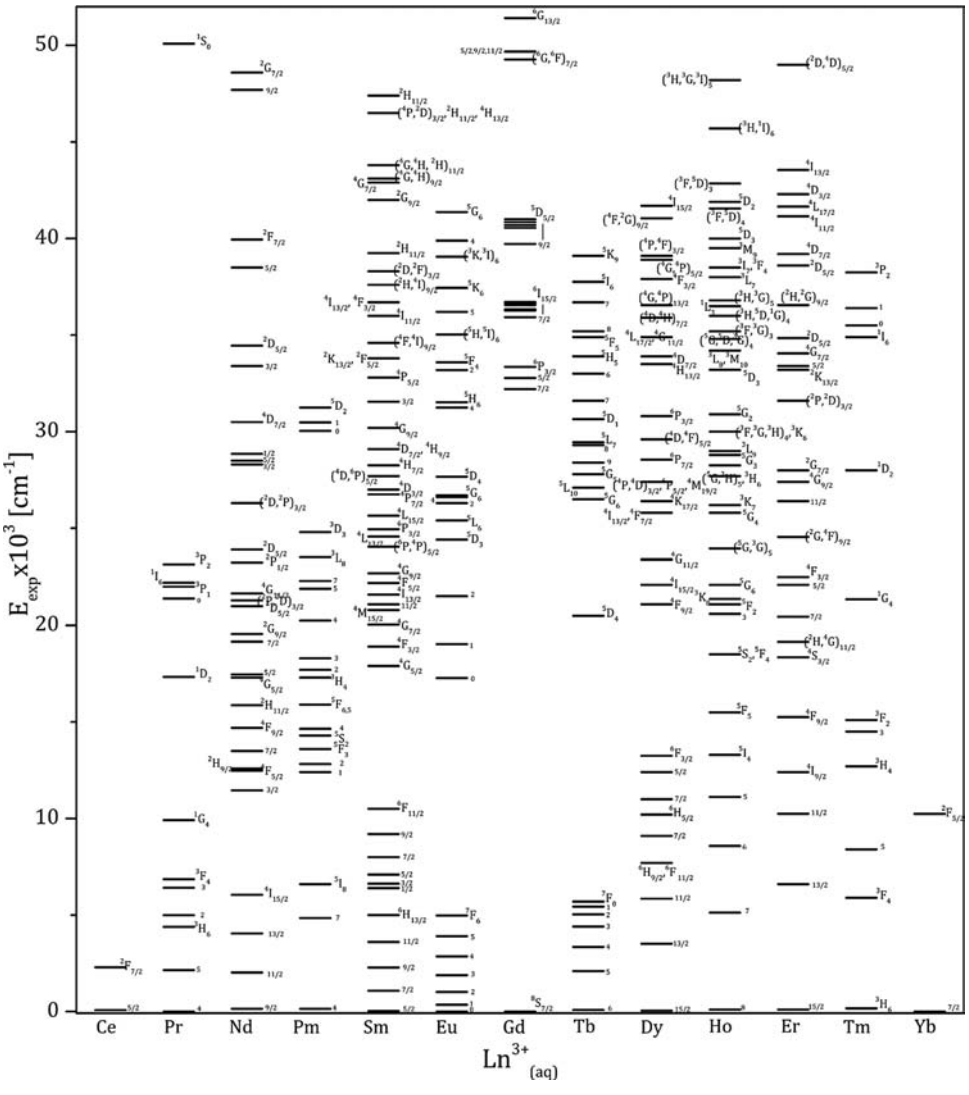

Figure 1.2 *Diagram of energy levels with corresponding term symbols for Ln(III) [16]*

1.3 The Nature of the *f-f* Transitions

1.3.1 Hamiltonian in Central Field Approximation and Coulomb Interactions

The behaviour of an electron is described by the wave function ψ, which is a solution of the Schrödinger equation 1.1.

$$H\psi = E\psi \tag{1.1}$$

This equation only has an exact solution for systems with one electron, but for polyelectronic systems with N electrons, the solution can be approximated by considering that each

electron is moving independently in a central spherically symmetric field $U(r_i)/e$ of the averaged potentials of all other electrons [6]. The Hamiltonian H_{CFA} for this central field approximation is shown in Equation 1.2.

$$H_{CFA} = \sum_{i=1}^{N} \left[\frac{-\hbar^2}{2m} \nabla^2 + U(r_i) \right] \tag{1.2}$$

$\hbar$ is the reduced Planck constant, m the mass and the Laplace operator is given by Equation 1.3.

$$\nabla^2 = \frac{\partial^2}{\partial x^2} + \frac{\partial^2}{\partial y^2} + \frac{\partial^2}{\partial z^2} \tag{1.3}$$

The Schrödinger equation can thus be written as shown in Equation 1.4.

$$\sum_{i=1}^{N} \left[\frac{-\hbar^2}{2m} \nabla^2 + U(r_i) \right] \Psi = E_{CFA} \Psi \tag{1.4}$$

In the central field approximation, solutions can be chosen such that the overall wavefunction and energy of the system are sums of wavefunctions and energies of one-electron systems, as shown in Equation 1.5.

$$\Psi = \sum_{i=1}^{N} \psi_i(a^i) \tag{1.5a}$$

$$E_{CFA} = \sum_{i=1}^{N} E_i \tag{1.5b}$$

a^i stands for the quantum numbers n, l and m_l which describe the state of the electron in the central field. By introducing the polar coordinates r, θ and ϕ instead of the Cartesian coordinates x, y and z, one can separate each one-electron wave function into its radial R_{nl} and angular Y_{lm_l} components, as shown in Equation 1.6.

$$\psi_i(a^i) = \frac{1}{r} R_{nl}(r) Y_{lm_l}(\theta, \phi) \tag{1.6}$$

Since R_{nl} is a function of r only, it depends on the central field potential $U(r_i)$. A solution to this wave function, shown in Equation 1.7, is approximated and depends on the form of the central field.

$$R_{nl}(r) = -\left[\left(\frac{2Z}{na_0} \right)^3 \frac{(n-l-1)!}{2n\{n+l\}^3} \right]^{1/2} e^{-\frac{\rho}{2}} \rho^l L_{n+l}^{2l+1}(\rho) \tag{1.7}$$

with $\rho = \frac{2Z}{na_0} r$ and $a_0 = \frac{h^2}{4\pi^2 \mu e^2}$, where a_0 is the Bohr radius and μ the reduced mass. This expression also includes the Laguerre polynomials $L_{n+l}^{2l+1}(\rho)$ shown in Equation 1.8.

$$L_{n+l}^{2l+1}(\rho) = \sum_{k=0}^{n-l-1} (-1)^{k+1} \frac{\{(n+l)!\}^2}{(n-l-1-k)!(2l+1+k)!k!} \rho^k \tag{1.8}$$

The angular wave functions, which are Laplacian spherical harmonics, on the other hand, are similar to the one-electron wave function and can thus be solved. Their expression is given in Equation 1.9.

$$Y_{lm_l}(\theta, \phi) = (-1)^m \left[\frac{(2l+1)(l-|m_l|)!}{4\pi(l+|m_l|)!} \right]^{\frac{1}{2}} P_l^{m_l}(\cos\theta) e^{im_l\phi} \tag{1.9}$$

$P_l^{m_l}(\cos\theta)$ are the Legendre functions shown in Equation 1.10.

$$P_l^{m_l}(\cos\theta) = \frac{(1-\cos^2\theta)^{m_l/2}}{2^l l!} \frac{d^{m_l+l}}{d\cos^{m_l+l}\theta} (\cos^2\theta - 1)^l \tag{1.10}$$

Relativistic corrections to the Schrödinger equation lead to the introduction of a spin function $\delta(m_s, \sigma)$, where σ is a spin coordinate and m_s is the magnetic spin quantum number, to the one electron wave function in Equation 1.6, which then takes the shape shown in Equation 1.11.

$$\psi(n, l, m_l, m_s) = \delta(l, n, m_l, m_s) R_{nl}(r) Y_{lm_l}(\theta, \phi) \tag{1.11}$$

Equation 1.5a can now be rewritten as Equation (1.12).

$$\Psi = \sum_{i=1}^{N} \psi_i(\alpha^i) \tag{1.12}$$

While the two equations look similar, in Equation 1.12 α^i stands for the four quantum numbers n, l, m_l and m_s, which describe the state of each i of the N electrons. These permutate to generate equally valid states following Pauli's exclusion principle, to yield anti-symmetric wave functions in the central field, which are solutions to the Schrödinger equation (Equation 1.4).

The lack of perturbations to the Hamiltonian in the central field approximation results in high degeneracy D (Equation 1.13) of the f electron configurations.

$$D = \frac{(4l+2)!}{N!(4l+2-N)!} = \frac{14!}{N!(14-N)!} \qquad \text{for } l = 3 \tag{1.13}$$

The Hamiltonian for the perturbation introduced by the potential energy H_{pot} felt by all electrons in the field of the nucleus corrected for the central spherically symmetric field is given by Equation 1.14.

$$H_{pot} = \sum_{i=1}^{N} \left[-\frac{Ze^2}{r_i} - U(r_i) \right] \tag{1.14}$$

Ze is the nuclear charge, r_i the position coordinates of electron i and $U(r_i)$ the spherical repulsive potential of all other electrons experienced by electron i moving independently in the field of the nucleus.

The repulsive Coulomb energy between pairs of electrons is an important perturbation to the central field approximation and its Hamiltonian $H_{Coulomb}$ is given by Equation 1.15.

$$H_{Coulomb} = \sum_{i<j}^{N} \frac{e^2}{r_{ij}} \tag{1.15}$$

e is the charge of the electron and r_{ij} is the distance between electrons i and j.

By applying $H_{Coulomb}$ to the wave function of the unperturbed system, it can be shown that the electrostatic repulsion energy E_{ER} of the system is given by Equation 1.16.

$$E_{ER} = \sum_{k=2,4,6} f_k F^k \tag{1.16}$$

Here, k is an integer of values 2, 4 and 6, f_k are the coefficients representing the angular part of the wave function [29] and F^k are the electrostatic Slater two-electron radial integrals given by Equation 1.17.

$$F^k = (4\pi)^2 e^2 \int_0^\infty \int_0^\infty \frac{r_<^k}{r_>^{k+1}} R_{nl}^2(r_i) R_{n'l'}^2(r_j) r_i^2 r_j^2 dr_i dr_j \tag{1.17}$$

$r_<$ is the smaller and $r_>$ the larger of the values of r_i and r_j. F_k instead of the Slater integrals are often indicated, for which:

$$F_2 = F^2/225$$
$$F_4 = F^4/1089$$
$$F_6 = F^6/7361.64$$

In the case of hydrogenic wave functions the following relationships are valid [30].

$$F_4 = 0.145\, F_2 \qquad F_6 = 0.0164\, F_2$$

These show that the values of F_k decrease as k increases. Values of F_2 for the configurations f^2 to f^{13} are tabulated in Table 1.3 and show that they increase with increasing atomic number, as the inter-electronic repulsion is expected to increase.

The f_k angular coefficients are hydrogen-like and can be determined from

$$f_k = \frac{(2l+1)(l-|m_l|)!}{2(l+|m_l|)!} \frac{(2l'+1)(l'-|m_l'|)!}{2(l'+|m_l'|)!} \int_0^\pi \{P_l^{m_l}(\cos\theta_i)\}^2 P_0^k(\cos\theta_i) \sin\theta_i d\theta_i \times \int_0^\pi \{P_{l'}^{m_{l'}}(\cos\theta_i)\}^2 P_0^k(\cos\theta_i) \sin\theta_i d\theta_i \tag{1.18}$$

As above, $P_l^{m_l}$, $P_{l'}^{m_{l'}}$ and P_0^k are Legendre polynomials.

Table 1.3 *Comparison of the average magnitude of perturbations for transition metal and lanthanide ions in cm^{-1} [13]*

Valence configuration	$H_{Coulomb}$	H_{s-o}	H_{cf}
$3d^N$	70 000	500	15 000
$4d^N$	50 000	1000	20 000
$5d^N$	20 000	2000	25 000
$4f^N$	70 000	1500	500
$5f^N$	50 000	2500	2000

In addition to the Coulomb interactions of electron–electron repulsion and electron–nucleus attraction, further perturbations influence the energy levels of the lanthanide ions, such as the coupling of the spin and angular momenta, commonly designated spin–orbit coupling, the crystal field or Stark effect, and the interaction with a magnetic field or Zeeman effect, which will be described in the following sections.

As illustrated in Fig. 1.3, by comparison to electron–electron repulsion, which leads to energy splits on the order of $10^4\,cm^{-1}$, and spin–orbit coupling, with splits on the order of $10^3\,cm^{-1}$, the crystal field and Zeeman effects are small perturbations, resulting in energy level splitting on the order of $10^2\,cm^{-1}$ at the most [13]. The magnitude of these data compared to the *d* metals is shown comparatively in Table 1.4. In the case of transition metals, the crystal field splitting dominates the spin–orbit coupling. However, for lanthanide ions, the crystal field splitting is almost negligible. The spin–orbit coupling is of increasing

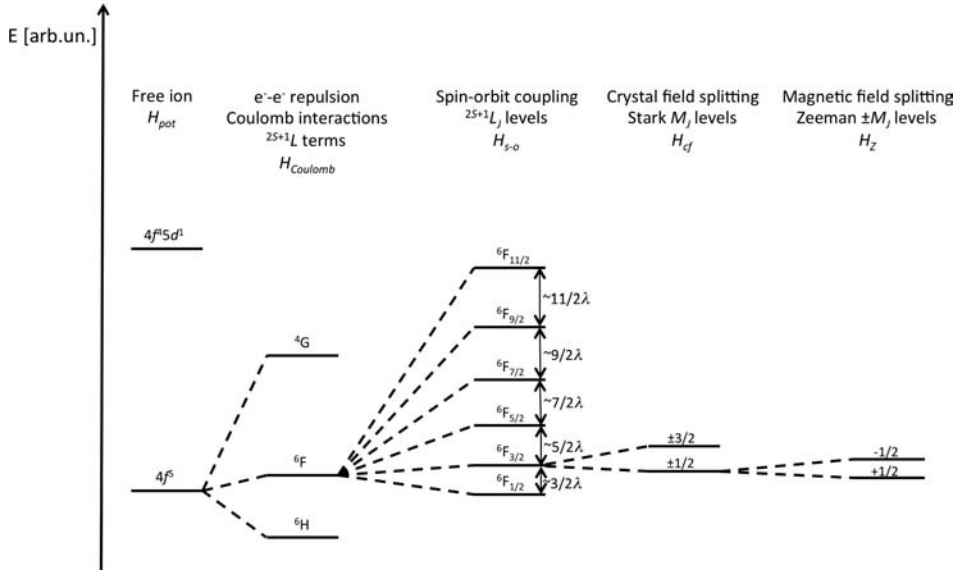

Figure 1.3 *Effect of the perturbations* [*Coulomb* ($H_{Coulomb}$), *spin–orbit* (H_{s-o}), *crystal field* (H_{cf}), *and magnetic field* (H_Z)] *on the electron configuration of an arbitrary Ln(III) Kramers' ion. Energy units are arbitrary and not to scale.* λ *is described in Section 3.2*

Table 1.4 *Spin–orbit radial integral ζ_{nl}, spin-orbit coupling constant λ and F_2 values for the $Ln^{3+}_{(aq)}$ ions [25–28,31]*

f^N	ζ_{nl} [cm^{-1}]	λ [cm^{-1}][a]	F_2 [cm^{-1}][b]
f^1	625	625	
f^2	740	370	305
f^3	884	295	321
f^4	1022	250	338
f^5	1157	231	364
f^6	1326	221	369
f^7	1450	0	384
f^8	1709	−285	401
f^9	1932	−386	407
f^{10}	2141	−535	419
f^{11}	2380	−793	440
f^{12}	2628	−1314	461
f^{13}	2870	−2880	444[c]

[a] f^1 as $Ce:LaCl_3$ [32] and f^{13} as $Yb_3Ga_5O_{12}$ [33].
[b] [16]
[c] [30]

importance for the heavier elements. However, in the case of the lanthanides, it is still approximately an order of magnitude smaller than the Coulomb interactions and one order of magnitude larger than the crystal field splitting; therefore an intermediate coupling scheme, in which *j-j* in addition to Russell–Saunders coupling is also important, is more correct. Nonetheless, as mentioned above, the latter formalism is utilised due to its simplicity.

1.3.2 Spin–Orbit Coupling

The spin and angular momenta of the individual electrons couple with each other and this coupling is increasingly important with atomic number. The Hamiltonian $H_{s\text{-}o}$ that describes this perturbation is given in Equation 1.19.

$$H_{s\text{-}o} = \sum_{i=1}^{N} \xi(r_i)(s_i \cdot l_i) \tag{1.19}$$

r_i is the position coordinate of electron i, and s_i and l_i are its spin and angular momentum quantum numbers. $\xi(r_i)$, the single electron spin–orbit coupling constant, is given by Equation 1.20.

$$\xi(r_i) = \frac{\hbar^2}{2m^2c^2r_i}\frac{dU(r_i)}{dr_i} \tag{1.20}$$

In this equation, c is the speed of light in a vacuum and $\hbar$ is the reduced Planck constant. $\xi(r_i)$ is related to the spin–orbit radial integral ζ_{nl} by equation 1.21.

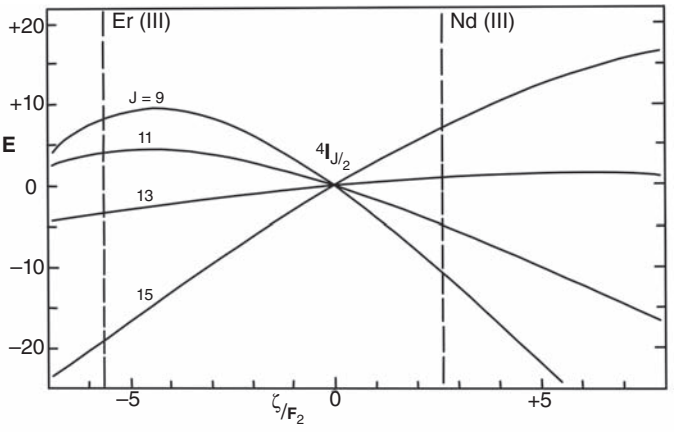

Figure 1.4 *The energies and splitting of the ^4I level for the f^3 and f^{11} configurations as a function of the ratio ζ_{nl}/F_2. The energy levels for the ratios −5.7 for Er(III) and 2.6 for Nd(III) are indicated by the dashed vertical lines. Adapted with permission from [16]. Interscience Publishers: New York, 1968*

$$\zeta_{nl} = \int_0^\infty R_{nl}^2 \xi(r) dr \tag{1.21}$$

and to the many electron spin–orbit coupling constant λ by Equation 1.22, for $S \neq 0$.

$$\lambda = \pm \frac{\xi(r)}{2S} \tag{1.22}$$

Values of ζ_{nl} and λ for the hydrated Ln^{3+} ions are summarised in Table 1.4, with λ positive for a more than half-filled shell and negative for a less than half-filled shell. It can be seen that ζ_{nl} increases with increasing number of f electrons, which corresponds to a higher atomic number Z and a stronger spin–orbit interaction, as expected.

$H_{s\text{-}o}$ will permit coupling of ^{2S+1}L states for $\Delta S \leq 1$ and $\Delta L \leq 1$. This effect is shown in Fig. 1.4, in which the energy splitting of the ^4I level due to spin–orbit coupling is shown as a function of the ratio ζ_{nl}/F_2. The increased curvature of the levels shows the increasing spin–orbit coupling. The energy levels of the reverse multiplet of Er(III) and of the multiplet of Nd(III) are indicated by the vertical dashed lines.

The calculated compositions of the ^4I multiplet levels of Nd(III) and of Er(III) are given below.

Nd(III)	Er(III)
$\langle {}^4I_{9/2} \vert = -0.166[^2H] + 0.984[^4I]$	$\langle {}^4I_{15/2} \vert = 0.982[^4I] - 0.186[^2K]$
$\langle {}^4I_{11/2} \vert = 0.995[^4I]$	$\langle {}^4I_{13/2} \vert = 0.995[^4I]$
$\langle {}^4I_{13/2} \vert = -0.993[^4I]$	$\langle {}^4I_{11/2} \vert = 0.133[^4G] - 0.129[^2H] + 0.442[^2H'] + 0.875[^4I]$
$\langle {}^4I_{15/2} \vert = 0.993[^4I] + 0.118[^2K]$	$\langle {}^4I_{9/2} \vert = -0.416[^4F] - 0.342[^2G] + 0.276[^2G'] - 0.219[^2H] + 0.438[^2H'] + 0.627[^4I]$

Here, $\langle {}^4I_J|$ is the wave function of the spin–orbit perturbed state and $[{}^4I]$ is the wave function of the unperturbed state; a state indicated by ' is a state with the same L and S but higher energy. Er(III), the heavier lanthanide ion, experiences a larger spin–orbit coupling, as can be seen from the graph as well as composition of the levels above. It can further be inferred that spin–orbit coupling leads to a splitting of the levels into terms with different J values. Diagonalisation of the energy matrix $\langle l^n \alpha LSJ | \sum_i \xi(r_i) s_i l_i | l^n \alpha' L' S' J' \rangle$ allows estimation of the energies of the split terms (Equation 1.23).

$$\begin{aligned} \langle l^n \alpha LSJ | \textstyle\sum_i \xi(r_i) s_i l_i | l^n \alpha' L' S' J' \rangle &= (-1)^{L+S'+j} \zeta_{nl} \sqrt{(2l+1)(l+1)} \delta_{JJ'} \\ &\times \begin{Bmatrix} L & S & J \\ S' & L' & 1 \end{Bmatrix} \langle l^n \alpha LS || V^{11} || l^n \alpha' L' S' \rangle \end{aligned} \tag{1.23}$$

δ_{ij} are the Kronecker delta symbols, for which $\delta_{ij} = 0$ for $i \neq j$ and $\delta_{ij} = 1$ for $i = j$. α stands for all additional quantum numbers which describe the initial and final states of l^n. The doubly reduced matrix elements $\langle l^n \alpha LS || V^{11} || l^n \alpha' L' S' \rangle$, containing the spin–orbit operator V^{11}, are tabulated [34]. The term between curly brackets is the six-j symbol, which describes the coupling of three momenta, in this case L, S and J. Online calculators are available to determine these, or they are tabulated [35]. From the 6-j symbol selection rules arise, as it is only non-zero when:

$$\Delta S = 0, \pm 1 \quad \Delta L = 0, \pm 1$$
$$S' + S \geq 1 \quad L' + L \geq 1$$
$$\Delta J = 0$$

The energy of each term with respect to the barycentre of the parent term ${}^{2S+1}L$ can be approximated by Equation 1.24.

$$E_J = {}^1\!/_2 \lambda [J(J+1) - L(L+1) - S(S+1)] \tag{1.24}$$

Using this equation, it is possible to estimate that the ${}^3H_5$ energy level of Pr^{3+} ($4f^2$) will be located approximately 370 cm^{-1} or -1λ below the barycentre of the ${}^3H$ level, while the ${}^3H_6$ will be 6λ or 2220 cm^{-1} above and the ${}^3H_4$ level -5λ or 1850 cm^{-1} below [16]. From Equation 1.24 it can further be concluded that the energy gap ΔE between two adjacent levels with $J' = J + 1$ is approximated by Landé's interval rule (see also Fig. 1.3), given in Equation 1.25.

$$\Delta E = \lambda J' \tag{1.25}$$

Landé's interval rule is only strictly obeyed in the case of strong LS coupling and is only approximated in lanthanides, where intermediate coupling, consisting of interaction of levels with the same J but different L and S, is more correct. As a consequence, the magnitude of the interval ΔE determined through Equation 1.25 is usually more accurate for the lower energy levels of the lighter lanthanides. Nonetheless, a good approximation between the experimentally observed gaps and the gaps calculated by Landé's rule is

usually seen, especially for ground-state multiplets. In the case of Pr^{3+} the free ion energy levels for $^3H_4$, $^3H_5$ and $^3H_6$ are located at 0, 2152 and 4389 cm^{-1}, respectively [16], leading to ΔE values of 2152 and 2237 cm^{-1} between $J = 4$ and 5 and $J = 5$ and 6, which reasonably approximate the values of 1850 and 2220 cm^{-1} obtained through Equation 1.25.

1.3.3 Crystal Field or Stark Effects

When lanthanide ions are in inorganic lattices or compounds in general, in addition to the Coulomb interactions and the spin–orbit coupling, each electron i also feels the effect of the crystal field generated by the ligands surrounding the metal ion, in analogy to the effect first described by Stark of an electric field on the lines of the hydrogen spectrum [36]. This perturbation lifts the $2J + 1$ degeneracy and generates new levels with M_J quantum numbers. Since a potential is generated by the electrons of the N ligands, which is felt by the electrons of the lanthanide ions, the Hamiltonian can be defined by Equation 1.26.

$$H_{cf} = -e \sum_1^N V(r_i) \tag{1.26}$$

e is the elementary charge, $V(r_i)$ is the potential felt by electron i and r_i its position. Following the same reasoning utilised to derive Equations 1.6 and 1.12 one can express the Hamiltonian as a function of the crystal field parameters B_q^k, which are related to the spherical harmonics Y_q^k, as shown in Equation 1.27 [37].

$$H_{cf} = \sum_{i,j,k} \left(B_q^k\right)(C_q^k)_i \tag{1.27}$$

The relationships between B_q^k and Y_q^k are shown in Equation 1.28.

$$\begin{aligned} B_0^k &= \int_0^\infty R_{nl}^2(r) r^k dr \sqrt{\frac{4\pi}{2k+1}} Y_0^k \sum_L \frac{Z_L e^2}{R_L^{k+1}} \\ B_q^k &= \int_0^\infty R_{nl}^2(r) r^k dr \sqrt{\frac{4\pi}{2k+1}} Re\ Y_q^k \sum_L \frac{Z_L e^2}{R_L^{k+1}} \\ B_q'^k &= \int_0^\infty R_{nl}^2(r) r^k dr \sqrt{\frac{4\pi}{2k+1}} Im\ Y_q^k \sum_L \frac{Z_L e^2}{R_L^{k+1}} \end{aligned} \tag{1.28}$$

L are the ligands responsible for the crystal field at a distance R_L, Z their charge and e the elementary charge. Often, instead of B_q^k, the equivalent structural parameters A_k^q are utilised as shown below.

$$B_q^k = a \times A_k^q \left\langle r^k \right\rangle \tag{1.29}$$

Table 1.5 *Expectation values $\langle r^k \rangle$ in a.u. [38]*

	$\langle r^1 \rangle$	$\langle r^2 \rangle$	$\langle r^3 \rangle$	$\langle r^4 \rangle$	$\langle r^5 \rangle$	$\langle r^6 \rangle$
Ce^{3+}	0.97	1.17	1.73	3.08	6.44	15.55
Pr^{3+}	0.93	1.08	1.55	2.65	5.36	12.53
Nd^{3+}	0.90	1.01	1.39	2.31	4.53	10.31
Sm^{3+}	0.84	0.89	1.15	1.81	3.38	7.32
Eu^{3+}	0.82	0.84	1.06	1.62	2.96	6.28
Gd^{3+}	0.79	0.79	0.98	1.46	2.61	5.45
Tb^{3+}	0.77	0.75	0.91	1.33	2.33	4.76
Dy^{3+}	0.75	0.71	0.84	1.21	2.08	4.19
Ho^{3+}	0.74	0.68	0.79	1.11	1.87	3.71
Er^{3+}	0.72	0.65	0.74	1.02	1.69	3.31
Tm^{3+}	0.70	0.62	0.69	0.94	1.54	2.97
Yb^{3+}	0.69	0.60	0.65	0.87	1.40	2.67

a is a constant for each B_q^k and A_k^q pair [29], and $\langle r^k \rangle$ represents the average or expectation value of r^k, where r is the nucleus–electron distance of the lanthanide ion, given by

$$\langle r^k \rangle = \int_0^\infty R_{nl}^2(r) r^k dr \tag{1.30}$$

Tabulated values of $\langle r^k \rangle$ for all Ln^{3+} are summarised in Table 1.5.

$(C_q^k)_i$ are the related tensor operators, which transform as the spherical harmonics and are given by

$$(C_q^k)_i = \sqrt{\frac{4\pi}{2k+1}} Y_q^k(i) \tag{1.31}$$

1.3.4 The Crystal Field Parameters B_q^k and Symmetry

The integer k runs in the range 0–7 and the parameters containing even values of k are responsible for the crystal field splitting, while those with odd values influence the intensity of the induced electronic dipole transitions (see Section 1.3.10 for more details) [8,9]. q is also an integer and its values depend on the symmetry of the crystal field and the magnitude of k, since $|q| \leq k$. The possible combinations of k and q for the crystal field parameters are given in Table 1.6 and the symmetry elements contained in the crystal field parameters are summarised in Table 1.7.

The B_0^0 coefficient is notably absent from these tables; since it is spherically symmetric, it acts equally on all f^N configurations. In energy level calculations it can therefore be incorporated into all spherically symmetric interactions and does not need to be considered individually.